International Journal of Numerical Methods for Heat & Fluid Flow

State estimation problems in PRF-shift magnetic resonance thermometry

César Pacheco, Helcio R.B. Orlande, Marcelo Colaco, George S. Dulikravich,

State estimation problems in PRF-shift magnetic resonance thermometry

César Pacheco, Helcio R.B. Orlande and Marcelo Colaco
Department of Mechanical Engineering, Universidade Federal do Rio de Janeiro, Rio de Janeiro, Brazil, and

George S. Dulikravich
Department of Mechanical and Materials Engineering, MAIDROC Lab., Florida International University, Miami, Florida, USA

Received 30 October 2016
Revised 6 June 2017
Accepted 10 June 2017

Abstract

Purpose – The purpose of this paper is to apply the Steady State Kalman Filter for temperature measurements of tissues via magnetic resonance thermometry. Instead of using classical direct inversion, a methodology is proposed that couples the magnetic resonance thermometry with the bioheat transfer problem and the local temperatures can be identified through the solution of a state estimation problem.

Design/methodology/approach – Heat transfer in the tissues is given by Pennes' bioheat transfer model, while the Proton Resonance Frequency (PRF)-Shift technique is used for the magnetic resonance thermometry. The problem of measuring the transient temperature field of tissues is recast as a state estimation problem and is solved through the Steady-State Kalman filter. Noisy synthetic measurements are used for testing the proposed methodology.

Findings – The proposed approach is more accurate for recovering the local transient temperatures from the noisy PRF-Shift measurements than the direct data inversion. The methodology used here can be applied in real time due to the reduced computational cost. Idealized test cases are examined that include the actual geometry of a forearm.

Research limitations/implications – The solution of the state estimation problem recovers the temperature variations in the region more accurately than the direct inversion. Besides that, the estimation of the temperature field in the region was possible with the solution of the state estimation problem via the Steady-State Kalman filter, but not with the direct inversion.

Practical implications – The recursive equations of the Steady-State Kalman filter can be calculated in computational times smaller than the supposed physical times, thus demonstrating that the present approach can be used for real-time applications, such as in control of the heating source in the hyperthermia treatment of cancer.

Originality/value – The original and novel contributions of the manuscript include: formulation of the PRF-Shift thermometry as a state estimation problem, which results in reduced uncertainties of the temperature variation as compared to the classical direct inversion; estimation of the actual temperature in the region with the solution of the state estimation problem, which is not possible with the direct inversion that is limited to the identification of the temperature variation; solution of the state estimation problem with the Steady-State Kalman filter, which allows for fast computations and real-time calculations.

Keywords Bioheat transfer, State estimation, Kalman filter, Inverse problems, Magnetic resonance thermometry

Paper type Research paper

This work was supported by Conselho Nacional de Desenvolvimento Científico e Tecnológico (CNPq) Coordenação de Aperfeiçoamento de Pessoal de Nível Superior (CAPES) Fundação Carlos Chagas Filho de Amparo a Pesquisa do Estado do Rio de Janeiro (FAPERJ) and Programa de Recursos Humanos da Agência Nacional de Óleo, Gás Natural e Biocombustíveis [ANP/PRH37].

International Journal of Numerical Methods for Heat & Fluid Flow
Vol. 28 No. 2, 2018
pp. 315-335

0961-5539
DOI 10.1108/HFF-10-2016-0427

Nomenclature

B_0 = external magnetic field, T;
c_b = blood specific heat at constant pressure, $Jkg^{-1}\,°C^{-1}$;
c_p = tissue specific heat at constant pressure, $Jkg^{-1}\,°C^{-1}$;
g_m = volumetric rate of heat generation due to metabolism, Wm^{-3};
g_h = volumetric rate of heat generation imposed by an external source, Wm^{-3};
h = convective heat transfer coefficient, $Wm^{-2}\,°C^{-1}$;
$\mathbf{H}$ = observation matrix;
k = thermal conductivity, $Wm^{-1}°\,C^{-1}$;
$\mathbf{P}$ = covariance matrix of the estimated state variables, $°C^2$;
$\mathbf{Q}$ = covariance matrix of the Gaussian noise of the evolution model, $°C^2$;
$\mathbf{R}$ = covariance matrix of the Gaussian noise of the observation model, $degree^2$;
$\mathbf{r}$ = position vector, m;
T = temperature, °C;
T_a = arterial blood temperature, °C;
t = time, s;
t_{TE} = echo time, s;
$\mathbf{w}$ = noise vector for the state variables, °C;
$\hat{\mathbf{x}}$ = estimated state variables, °C;
$\mathbf{v}$ = noise vector for the observations, degree; and
V = volume, m^3.

Greek symbols

α = PRF-shift coefficient, ppm $°C^{-1}$;
δ = phase shift, see equation (9.b), degree;
ΔT = temperature variation, °C;
Δt = time step, s;
$\partial\Omega$ = boundary of the physical domain;
γ = gyromagnetic ratio, degree $s^{-1}T^{-1}$;
Φ = phase, degree;
ω = blood perfusion rate in the tissue, s^{-1};
Ω = physical domain;
ρ = density, kgm^{-3};
ρ_b = blood density, kgm^{-3};
σ_δ = standard deviation of the phase shift, degree; and
$\sigma_{\Delta T}$ = standard deviation of the temperature variation, °C.

Subscripts

n = time t_n

Superscripts

$+$ = posterior; and
$-$ = prior.

Introduction

One of the main research topics in the area of cancer treatment has been the development of protocols that are minimally invasive or not invasive at all. This kind of treatment has several advantages, including minor risks of post-surgical complications, patient's shorter recovering time and smaller total operation costs (Hynynen *et al.*, 1996). In fact, non-invasive

treatments, like radiotherapy, have been commonly used in practice. A promising non-invasive cancer treatment that has been drawing a lot of attention recently is hyperthermia, where the temperature of the neoplastic tissue is increased to induce cell necrosis (in this case, hyperthermia is referred to as thermo-ablation) or improve the sensitivity of the cells to cytotoxic agents, like chemotherapeutic drugs or radiation (Rieke and Butts Pauly, 2008). An important requirement for the hyperthermia treatment of cancer is to limit thermal damage to the cancerous cells, without affecting the surrounding healthy tissues. Recent technological advances in nanotechnology allowed that nanoparticles, which act as strong absorbers of electromagnetic waves, be concentrated inside the tumors, thus providing local heating in the region of interest (Bayazitoglu, 2009; Bayazitoglu *et al.*, 2013; Dombrovsky *et al.*, 2011; Dombrovsky *et al.*, 2015).

Hyperthermia protocols require the accurate real-time information about the local temperatures inside the body, especially in the region containing the tumor, where healthy cells are most likely to be thermally damaged. State estimation problems have been successfully used to recover the temperature inside the body for hyperthermia treatments, by using simulated measurements of one single temperature sensor inside the domain (Varon *et al.*, 2015; Varon *et al.*, 2016; Lamien *et al.*, 2016, 2017). However, these works did not deal with the practical aspects of the temperature measurement, which is the main focus of this paper.

Magnetic resonance thermometry (MRT) has been a topic of research for several years now (de Senneville *et al.*, 2005; Rieke and Butts Pauly, 2008). Among the different MRT techniques available in the literature, the most widely used is the so-called PRF-Shift method (PRF is the acronym for *Proton Resonance Frequency*), which was developed by Ishihara *et al.* (1995). The temperature measurements obtained with the PRF-Shift method involve smaller variances than those obtained with other MRT methods (Wlodarczyk *et al.*, 1998). Several works can be found in the literature with the application of the PRF-Shift method to hyperthermia, by using the direct inversion of the magnetic resonance measurements to recover the temperatures (Mougenot *et al.*, 2009; Salomir *et al.*, 2000a, 2000b, 2003; Weidensteiner *et al.*, 2004; Mougenot *et al.*, 2004). Data acquisition systems, which include data interpolation for the filtering of noise, have also been developed to obtain more accurate temperature measurements with the PRF-Shift method (Yang *et al.*, 1998; De Zwart *et al.*, 1999; Salomir *et al.*, 2000a, 2000b; Kuroda *et al.*, 2000; Rieke *et al.*, 2004; Kuroda *et al.*, 2006; Langley *et al.*, 2011). Differently from the above works, in the present paper, the transient temperature field in the region of interest is recovered through the solution of a state estimation problem (Doucet *et al.*, 2001; Arulampalam *et al.*, 2002; Chen, 2003; Kaipio and Somersalo, 2004; Simon, 2006; Orlande *et al.*, 2012), which can cope with uncertainties in the evolution and measurement models, thus reducing inaccuracies and instabilities inherent to the direct inversion of the magnetic resonance data. The state estimation problem is solved with an asymptotic version of the Kalman filter, referred to as Steady-State Kalman Filter (SSKF; Simon, 2006; Pacheco *et al.*, 2016), which does not require the recursive calculation of several matrices for the implementation of the method. Therefore, the SSKF involves computational times of the same order of those required for the direct inversion, but results in more accurate temperatures in the region because it is coupled to a bioheat transfer model. Furthermore, with the present approach, the actual temperature in the region can be recovered, while only the temperature variation can be obtained with the direct inversion of the magnetic resonance data. Two-dimensional idealized cases are solved here with simulated measurements, to demonstrate the capabilities of the proposed approach to indirectly measure the temperature in the region by solving a state estimation problem.

Physical problem and mathematical formulation

Different bioheat transfer models (Fan and Wang, 2011; Fiala *et al.*, 2012) have been developed after the pioneering work of Pennes (1948). Despite the limitations in Pennes' model, which does not take into account changes in the arterial blood temperature, there is still no model proven to be sufficiently general and valid for different organs or tissues. In fact, even a pure heat conduction model has been used for tissues with low blood perfusion (Dombrovsky *et al.*, 2015). Since the main objective of this work is to obtain the temperature measurement with the PRF-Shift method through the solution of a state estimation problem, Pennes' classical model is used here.

In the physical problem under analysis, the spatial domain Ω, initially at the temperature $T_0(\mathbf{r})$, is externally heated for the hyperthermia treatment. The external heating results in a volumetric heat source rate, $g_h(\mathbf{r},t)$. The surface $\partial\Omega$ of Ω exchanges heat by convection and linearized radiation with the surrounding environment at the temperature T_∞ with a heat transfer coefficient h. The formulation of this problem in terms of Pennes' model is given by:

$$\rho(\mathbf{r})c_p(\mathbf{r})\frac{\partial T}{\partial t} = \nabla\cdot[k(\mathbf{r})\nabla T] + \omega(\mathbf{r})\rho_b c_b[T_a - T(\mathbf{r},t)] + g_h(\mathbf{r},t) + g_m(\mathbf{r}), \quad \mathbf{r}\in\Omega,\ t>0 \tag{1.a}$$

$$k(\mathbf{r})\frac{\partial T}{\partial \mathbf{n}} + hT = hT_\infty, \qquad \mathbf{r}\in\partial\Omega,\ t>0 \tag{1.b}$$

$$T(\mathbf{r},t) = T_0(\mathbf{r}), \qquad \mathbf{r}\in\Omega,\ t=0 \tag{1.c}$$

where the tissues' thermophysical properties, as well as the metabolic heat generation, $g_m(\mathbf{r})$, are allowed to vary spatially.

For convenience in the analysis related to the PRF-Shift thermometry, the temperature $T(\mathbf{r},t)$ is written in terms of the initial temperature in the region before the external heating is imposed, $T_0(\mathbf{r})$, and the temperature variation due to the heating, $\Delta T(\mathbf{r},t)$, that is:

$$T(\mathbf{r},t) = T_0(\mathbf{r}) + \Delta T(\mathbf{r},t) \tag{2}$$

Here, $T_0(\mathbf{r})$ is the solution of the steady state version of problem (1) without the external heating (that is, $g_h(\mathbf{r},t) = 0$), which is given by:

$$\nabla\cdot[k(\mathbf{r})\nabla T_0(\mathbf{r})] + \omega(\mathbf{r})\rho_b c_b[T_a - T_0(\mathbf{r})] + g_m(\mathbf{r}) = 0, \quad \mathbf{r}\in\Omega \tag{3.a}$$

$$k(\mathbf{r})\frac{\partial T_0(\mathbf{r})}{\partial \mathbf{n}} + hT_0(\mathbf{r}) = hT_\infty, \qquad \mathbf{r}\in\partial\Omega \tag{3.b}$$

By substituting equation (2) into equations (1.a-c) and taking into account problem equations (3.a,b), the following problem for the temperature variation $\Delta T(\mathbf{r},t)$ can be obtained:

$$\rho(\mathbf{r})c_p(\mathbf{r})\frac{\partial \Delta T}{\partial t} = \nabla\cdot\left[k(\mathbf{r})\nabla(\Delta T)\right] - \omega\rho_b c_b\Delta T(\mathbf{r},t) + g_h(\mathbf{r},t), \quad \mathbf{r}\in\Omega,\ t>0 \tag{4.a}$$

$$k(\mathbf{r})\frac{\partial \Delta T}{\partial \mathbf{n}} + h\Delta T(\mathbf{r},t) = 0, \qquad \mathbf{r} \in \partial\Omega,\ t > 0 \tag{4.b}$$

$$\Delta T(\mathbf{r},t) = 0, \qquad \mathbf{r} \in \Omega,\ t = 0 \tag{4.c}$$

Several methods can be found in the literature to measure the temperature non-invasively by means of magnetic resonance, but the most widely used is the PRF-Shift method introduced by Ishihara *et al.* (1995). This method has shown, throughout the years, to be capable of providing more reliable and robust measurements than other available ones (Wlodarczyk *et al.*, 1998; Quesson *et al.*, 2000; Rieke and Butts Pauly, 2008).

Magnetic resonance imaging techniques are based on the application of a constant and homogeneous magnetic field, $\mathbf{B}_0$, with magnitude B_0, to the subject under analysis. This magnetic field suffers a slight perturbation in the vicinity of the atomic nucleus, due to the movement of the electrons around the nucleus, which is proportional to the external magnetic field vector $\mathbf{B}_0$. Thus, the magnetic field is sensed by the atomic nucleus according to:

$$B(\mathbf{r}) = [1 - s(\mathbf{r})]B_0 \tag{5}$$

where $s(\mathbf{r})$ is the *chemical shift* (Brown *et al.*, 1999; Kuperman, 2000).

The magnetic dipoles of each atom tend to align with the external magnetic field $\mathbf{B_0}$. This behavior is described by the Bloch equations (Bloch, 1946) and the practical result is that the net magnetization vector, $\mathbf{M}$ (i.e. the sum of the magnetization vector of each individual atom), oscillates around $\mathbf{B}_0$ (Figure 1) with the angular velocity:

$$\omega(\mathbf{r}) = \gamma B(\mathbf{r}) = \gamma[1 - s(\mathbf{r})]B_0 \tag{6}$$

where γ is the gyromagnetic ratio (Brown *et al.*, 1999).

The PRF-Shift method is based on the temperature sensitivity of the chemical shift, that is, $s(\mathbf{r}) \equiv s(\mathbf{r},T)$. The chemical shift is proportional to the local temperature, that is, there exists a linear relationship between the local magnetic field and the local temperature, so that we can write (de Senneville *et al.*, 2005; Rieke and Butts Pauly, 2008):

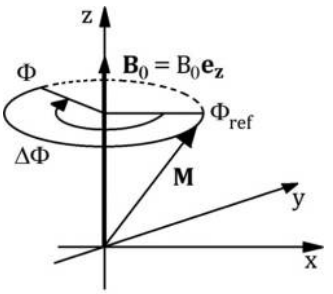

Source: Modified from Kuperman (2000)

Figure 1.
Oscillation of the global magnetization vector **M** around the axis of the external magnetic field $\mathbf{B_0}$

$$\frac{\partial s(\mathbf{r}, T)}{\partial T(\mathbf{r})} = \alpha \tag{7}$$

where α was shown to be practically independent of the tissue type, except for fat (de Senneville *et al.*, 2005; Rieke and Butts Pauly, 2008). This is a clear advantage of the PRF-Shift method, since other MRT methods are strongly affected by the tissue type (Rieke and Butts Pauly, 2008).

The local phase shift, $\Delta\Phi(\mathbf{r},T)$ (Figure 1), can be calculated from equation (6) as (De Poorter *et al.*, 1994):

$$\Delta\Phi(\mathbf{r}, T) = \Phi(\mathbf{r}, T) - \Phi_{ref}(\mathbf{r}) = \gamma[1 - s(\mathbf{r}, T)]B_0\Delta t, \tag{8}$$

Here, $\Phi_{ref}(\mathbf{r})$ is a reference phase value and Δt is the time interval at the end of which the phase shift $\Delta\Phi(\mathbf{r},T)$ is measured in the magnetic resonance device. This time interval is typically called echo-time and it is represented by t_{TE} (Brown *et al.*, 1999). Equation (8) is written for the initial temperature $T_0(\mathbf{r})$ and for another general temperature $T(\mathbf{r},t) = T_0(\mathbf{r}) + \Delta T(\mathbf{r},t)$; thus, by taking into account equation (7), $\Phi_{ref}(\mathbf{r})$ is eliminated from the two equations to yield:

$$\Delta T(\mathbf{r}, t) = -\frac{\delta(\mathbf{r}, T)}{\alpha\gamma B_0 t_{TE}} \tag{9.a}$$

$$\text{where} \quad \delta(\mathbf{r}, T) = \Phi(\mathbf{r}, T) - \Phi(\mathbf{r}, T_0) \tag{9.b}$$

Equation (9) provides a relation between the temperature variation and the resulting phase variation. Therefore, from the magnetic resonance measurements of $\Phi(\mathbf{r},T) - \Phi(\mathbf{r},T_0)$, the temperature variation can be directly inferred from equation (9). Since the dynamics of the magnetic resonance measurements are much faster than that of the bioheat transfer, equation (9) can be sequentially applied to recover the transient temperature variation that is the solution of equation (4). This *direct inversion* is commonly used in practice for measuring temperature variations with the PRF-Shift method (Rieke *et al.*, 2004; Mougenot *et al.*, 2004; Kuroda *et al.*, 2006; Langley *et al.*, 2011; Fite *et al.*, 2012). To avoid that uncertainties in the measurements of $\Phi(\mathbf{r},T) - \Phi(\mathbf{r},T_0)$ be directly propagated to the temperature variation $\Delta T(\mathbf{r},t)$, a state estimation problem is solved in this work as described next.

State estimation problem

State estimation problems aim at obtaining information about dynamic variables that define the state of a system (state variables), by using transient measurements of some response of the system, as well as the information provided by a stochastic model for the evolution of the state variables (evolution model) and by a stochastic model that relates the measurements to the state variables (observation model) (Doucet *et al.*, 2001; Arulampalam *et al.*, 2002; Chen, 2003; Kaipio and Somersalo, 2004; Simon, 2006; Orlande *et al.*, 2012). State estimation problems are sequentially solved within the Bayesian framework, as time evolves and new measured data becomes available. By denoting the vector of state variables by $\mathbf{x}$ and the vector of measurements by $\mathbf{y}$, Bayes' theorem is written as (Kaipio and Somersalo, 2004):

$$\pi(\mathbf{x}|\mathbf{y}) = \frac{\pi(\mathbf{y}|\mathbf{x})\pi(\mathbf{x})}{\pi(\mathbf{y})} \tag{10}$$

Here, $\pi(\mathbf{x}|\mathbf{y})$ is the posterior probability density function, $\pi(\mathbf{y}|\mathbf{x})$ is the likelihood, $\pi(\mathbf{x})$ is the prior and $\pi(\mathbf{y})$ plays the role of a normalizing constant.

In this work, the vector of state variables, $\mathbf{x}$, contains the values of the local temperature variation, while $\mathbf{y}$ contains the phase shift measurements, that is:

$$\mathbf{x}_n = \Delta\mathbf{T}_n \tag{11.a}$$

$$\mathbf{y}_n = \boldsymbol{\delta}_n \tag{11.b}$$

where the subscript n refers to these variables at time t_n.

In cases where the evolution and observation models are linear and with additive Gaussian uncertainties in the form:

$$\mathbf{x}_n = \mathbf{F}_{n-1}\mathbf{x}_{n-1} + \mathbf{w}_n \tag{12.a}$$

$$\mathbf{y}_n = \mathbf{H}_n\mathbf{x}_n + \mathbf{v}_n \tag{12.b}$$

the optimal method for the solution of the state estimation problem is the Kalman filter (Kalman, 1960; Ho and Lee, 1964; Chen, 2003; Kaipio and Somersalo, 2004; Grewal and Andrews, 2008; Orlande, 2010; Orlande *et al.*, 2012). In equations (12.a,b), the random vectors $\mathbf{w}$ and $\mathbf{v}$ represent the noise in the evolution and observation models, which are assumed with zero means and known covariance matrices $\mathbf{Q}_n$ and $\mathbf{R}_n$, respectively.

In this work, the matrix $\mathbf{F}_{n\text{-}1}$ is obtained by the discretization of equations (4.a)-(4.c) with the Finite Volume Method (Patankar, 1980; Versteeg and Malalasekera, 1995), while the matrix $\mathbf{H}_n$ is obtained from equation (9) as:

$$\mathbf{H}_n = -\alpha\gamma t_{\mathrm{TE}} B_0 \mathbf{I} \tag{13}$$

The solution of the present state estimation problem is obtained by the Kalman filter recursive equations as (Kalman, 1960; Ho and Lee, 1964; Chen, 2003; Kaipio and Somersalo, 2004; Grewal and Andrews, 2008; Orlande, 2010; Orlande *et al.*, 2012):

$$\hat{\mathbf{x}}_{\mathrm{n}}^{-} = \mathbf{F}_{\mathrm{n-1}}\hat{\mathbf{x}}_{\mathrm{n-1}}^{+} \tag{14.a}$$

$$\mathbf{P}_{\mathrm{n}}^{-} = \mathbf{F}_{\mathrm{n}}\mathbf{P}_{\mathrm{n-1}}^{+}\mathbf{F}_{\mathrm{n}}^{\mathrm{T}} + \mathbf{Q}_{\mathrm{n}} \tag{14.b}$$

$$\mathbf{K}_{\mathrm{n}} = \mathbf{P}_{\mathrm{n}}^{-}\mathbf{H}_{\mathrm{n}}^{\mathrm{T}}\left[\mathbf{H}_{\mathrm{n}}\mathbf{P}_{\mathrm{n}}^{-}\mathbf{H}_{\mathrm{n}}^{\mathrm{T}} + \mathbf{R}_{\mathrm{n}}\right]^{-1} \tag{14.c}$$

$$\hat{\mathbf{x}}_{\mathrm{n}}^{+} = \hat{\mathbf{x}}_{\mathrm{n}}^{-} + \mathbf{K}_{\mathrm{n}}\left(\mathbf{y}_{\mathrm{n}} - \mathbf{H}_{\mathrm{n}}\hat{\mathbf{x}}_{\mathrm{n}}^{-}\right) \tag{14.d}$$

$$\mathbf{P}_{\mathrm{n}}^{+} = (\mathbf{I} - \mathbf{K}_{\mathrm{n}}\mathbf{H}_{\mathrm{n}})\mathbf{P}_{\mathrm{n}}^{-} \tag{14.e}$$

The estimation process is performed recursively (i.e. at each time step) in a two-step process. In the first step given by equations (14.a) and (14.b), the state variables are predicted with the application of the evolution model, resulting in a prior estimate $\hat{\mathbf{x}}_n^-$ for the state vector. In the second step, this prior estimate is corrected, yielding the posterior estimate $\hat{\mathbf{x}}_n^+$.

The Kalman filter is a very efficient and robust technique, resulting in unbiased estimates with minimum variance if the hypotheses of linear and Gaussian models apply (Chen, 2003; Grewal and Andrews, 2008). However, due to the matrix inversion in equation (14.c), the algorithm performs $O(n^3)$ floating point operations, where n is the number of state variables. Therefore, the large computational effort required for the application of the Kalman filter to problems with high spatial resolution, such as those demanded for the accurate control of the temperature field in multidimensional cases, may not allow the solution of the state estimation problem in real time for hyperthermia applications. On the other hand, for problems where the matrices $\mathbf{F}$, $\mathbf{H}$, $\mathbf{Q}$ and $\mathbf{R}$ do not evolve with time, that is, when:

$$\mathbf{F}_n = \mathbf{F}, \quad \mathbf{H}_n = \mathbf{H}, \quad \mathbf{Q}_n = \mathbf{Q}, \quad \mathbf{R}_n = \mathbf{R} \tag{15.a-d}$$

an approximation of the Kalman filter equations can be performed, resulting in the SSKF (Simon, 2006). Assuming that equations (15) hold, the prior and posterior estimates of the covariance matrices, $\mathbf{P}_n^-$ and $\mathbf{P}_n^+$, respectively, tend asymptotically to a constant matrix $\mathbf{P}_\infty$. In the SSKF, $\mathbf{P}_\infty$ is calculated directly and used as approximations for $\mathbf{P}_n^-$ and $\mathbf{P}_n^+$. This leads to a significant reduction in the number of computer operations at each time step because not only these matrices, but also the Kalman gain matrix, $\mathbf{K}$ (equation 14.c), can be calculated before the estimation process is applied.

The SSKF equations are given by (Simon, 2006):

$$\mathbf{P}_\infty = \mathbf{F}\mathbf{P}_\infty\mathbf{F}^T - \mathbf{F}\mathbf{P}_\infty\mathbf{H}^T\left(\mathbf{H}\mathbf{P}_\infty\mathbf{H}^T + \mathbf{R}\right)^{-1}\mathbf{H}\mathbf{P}_\infty\mathbf{F}^T + \mathbf{Q} \tag{16.a}$$

$$\mathbf{K}_\infty = \mathbf{P}_\infty\mathbf{H}^T\left(\mathbf{H}\mathbf{P}_\infty\mathbf{H}^T + \mathbf{R}\right)^{-1} \tag{16.b}$$

$$\hat{\mathbf{x}}_n^+ = (\mathbf{I} - \mathbf{K}_\infty\mathbf{H})\mathbf{F}\hat{\mathbf{x}}_{n-1}^+ + \mathbf{K}_\infty\mathbf{y}_n \tag{16.c}$$

Here, only equation (16.c) is calculated during the recursive estimation, being the calculation of equations (16.a) and (16.b) performed in a preprocessing step.

Equation (16.a) is a discrete Ricatti equation (Simon, 2006) and can be readily solved with different numerical libraries available in the literature. In this work, this equation was solved using the SLICOT library (Benner *et al.*, 1999). In comparison with the original Kalman filter, the SSKF requires, at each time step, only $O(n^2)$ floating point operations, thus allowing for a reduction of computational times.

Results

The application of the SSKF to the PRF-Shift method of temperature measurement with magnetic resonance, which is proposed here, was verified with two idealized numerical experiments, as described below. In the first numerical experiment, a square region with a uniform computational mesh was examined, while the second numerical experiment

dealt with an irregular region of the forearm that was discretized with an unstructured mesh.

Except for the Ricatti equation solver, the computer codes used herein were developed by the authors during this work. The codes were written in Fortran90 and compiled with gfortran. The computer codes were executed sequentially in an Intel® Core™ i7-2600CPU at 3.4 GHz computer, with 16 GB of RAM and Xubuntu 14.04.4 LTS operational system.

Square region

In this first numerical experiment, the domain was a square with dimensions 0.12 m × 0.12 m. The phase shift measurements were considered available over a 24 × 24 regular grid, but it was desired to estimate the temperature variation distribution in a more refined 48 × 48 grid. The external heating was idealistically assumed to be concentrated in a circular region, centered at $x = y = 0.06$ m and with radius of 0.025 m, with magnitude $g_h(\mathbf{r},t) = 5 \times 10^5$ W m^{-3} (Figure 2). This source term was constant until the maximum temperature variation in the domain reached 2.5°C and it was turned off afterward.

The noisy phase shift measurements were obtained synthetically, by solving the forward problem in the 48 × 48 grid and projecting the solution onto the 24 × 24 grid via local averaging. These temperature variations in the coarse grid were then transformed through (equation 9) into the phase shift values ($\mathbf{y}^e$) and the simulated measurements were obtained as:

$$\mathbf{y}_n = N\left(\mathbf{y}_n^e, \mathbf{R}\right) \tag{17}$$

In this work, both the state and observation noises were considered to be uncorrelated and with constant standard deviations, $\sigma_{\Delta T}$ and σ_δ, so that:

$$\mathbf{Q} = \sigma_{\Delta T}^2 \mathbf{I} \tag{18.a}$$

$$\mathbf{R} = \sigma_\delta^2 \mathbf{I} \tag{18.b}$$

Therefore, the noisy phase shift measurements were simulated by:

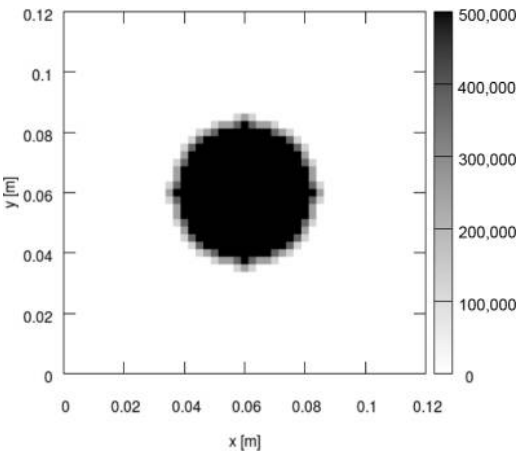

Figure 2.
Distribution of external heating $g_h(\mathbf{r}, t)$ represented on a 48 × 48 grid

$$\mathbf{y}_n = \mathbf{y}_n^e + \sigma_\delta \boldsymbol{\omega}; \tag{19}$$

where $\boldsymbol{\omega}$ is a random Gaussian vector with zero mean and identity covariance matrix. The standard deviation for the evolution model of the temperature variation $\sigma_{\Delta T}$ was taken as 0.05°C. The standard deviation of the phase shift (both for the measurements and for the observation model), σ_δ, was chosen to be 10 per cent of the maximum phase shift value observed during the simulations of the forward problem.

The magnetic resonance parameters used for this case were $\gamma = 1.53 \times 10^{10}$ degree $s^{-1}T^{-1}$, $t_{TE} = 18$ ms, $\alpha = -0.01$ ppm°C^{-1}, $B_0 = 1.5$T (Mougenot *et al.*, 2009), with the thermal properties of water ($\rho c_p = 4.180$ kJm^{-3} °C^{-1} and $k = 0.60$ Wm^{-1} °C^{-1}; Ozisik, 1985), $h = 10$ Wm^{-2} °C^{-1}, no perfusion and no metabolic heat generation. The experiment was numerically simulated until the final time of 600 s and the measurements were supposed available every time step $\Delta t = 0.1$ s.

The temperature variation obtained from the solution of the direct problem given by equations (4) are compared in Figure 3, for the 48 × 48 and 24 × 24 grids, at $t = 100$ s. A significant loss in spatial resolution can be noticed in Figure 3, due to the reduction of about 75 per cent in the number of pixels when the coarse (24 × 24) grid is used instead of the finer (48 × 48) uniform grid. Such reduced resolution directly affects the temperatures recovered from the direct inversion of equation (9), as presented by Figure 4, unless some image refinement technique is applied as postprocessing. A comparison of Figures 4 and 3.b reveals that, for the level of measurement error considered here, the direct inversion technique provides an accurate estimation for the temperature field in the region at $t = 100$ s, although some noise can be observed in Figure 4 at the regions not affected by the source term.

The noise observed with the direct inversion technique can be reduced with the application of the approach proposed here, based on the solution of a state estimation problem via the SSKF. Furthermore, the present approach allows the estimation of the state variables in a grid more refined than that of the measurements, without loss of accuracy. This is illustrated by Figure 5, which presents the temperatures estimated on a 48 × 48 grid with the phase-shift measurements over a 24 × 24 grid, at $t = 100$ s.

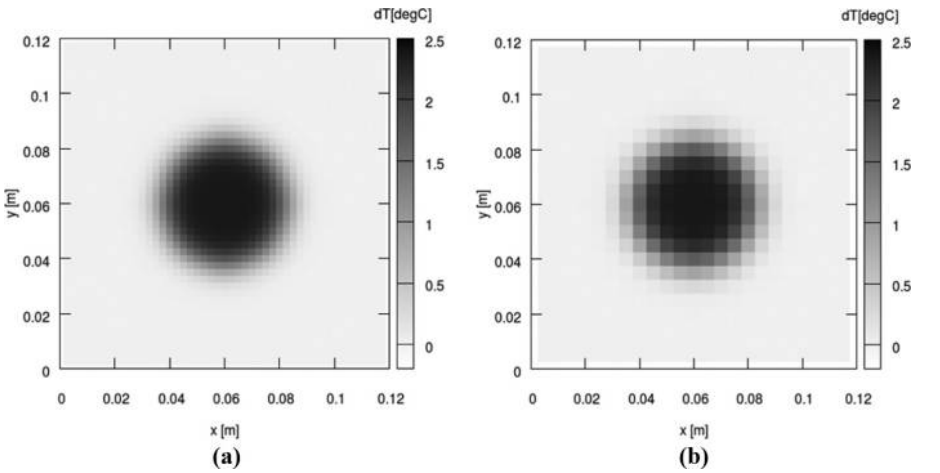

Figure 3.
Comparison between the forward problem solutions at $t = 100$ s: (a) 48 × 48 grid; (b) 24 × 24 grid

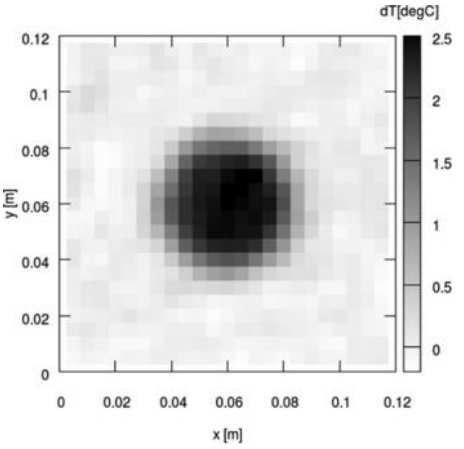

Figure 4.
Temperature variation at $t = 100$ s obtained via direct inversion on a 24×24 grid

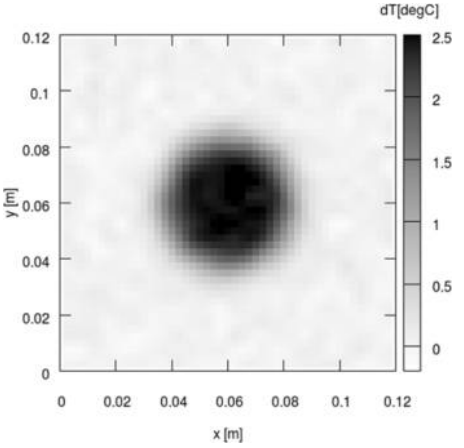

Figure 5.
Temperature variation at $t = 100$ s obtained via SSKF on a 48×48 grid

The more accurate results for a more refined grid, which were obtained with the SSKF than with the direct inversion, become more apparent when the time variation of the temperature variation at a specific point in the domain is examined, as presented by Figure 6. This figure shows the exact temperature variation at the center of the domain ($x = y = 0.06$ m), as well as temperature variations estimated with the direct inversion and the SSKF [Figure 6(a)], and the estimation errors (difference between estimated and exact temperature variations) obtained with these two methods [Figure 6(b)]. While the errors with the direct inversion frequently reach more than 0.5°C, the errors with the SSKF are at most 0.2°C except at the begin of the heating process. The larger errors observed with the SSKF for small times are due to the approximate asymptotic matrices used in the SSKF instead of the actual transient matrices of the classical Kalman filter. These larger errors, however, are still smaller than those observed with the direct inversion approach.

The recursive estimation through the SSKF took 20 s of computational time for this case, which involved a physical simulation time of 600 s. Hence, the proposed approach based on the solution of the state estimation problem with the SSKF can be used in real-time applications. A preprocessing step of approximately 10 min was necessary to solve Ricatti's equation (16.a). On the other hand, this preprocessing stage is completely independent of the recursive solution with the SSKF. The solution of the same state estimation problem using the classical Kalman filter took 30 min of computational time. Therefore, for this case, the SSKF was two orders of magnitude faster than the classical Kalman filter.

Human forearm region

In this second numerical experiment, a more realistic geometry was analyzed, involving a 2D transversal cut of a human right forearm; the geometry was obtained from the *Visible Human Dataset* project (Spitzer and Whitlock, 1998) and is presented by Figure 7(a). To solve the forward problem and calculate the **F** matrix for the Kalman filter, equations (4.a)-(4.c) were solved with the Finite Volume Method over an unstructured mesh, using a cross-diffusion correction term (Versteeg and Malalasekera, 1995; Mathur and Murthy, 1997). The numerical grid was generated with the software GMSH (Geuzaine and Remacle, 2009). The grid used for the analysis presented below, with approximately 6,000 control volumes, is shown in Figure 7(b). This number of control volumes was selected based on a grid convergence analysis and the numerical solution of the forward problem obtained with finite volumes was verified against the results obtained with COMSOL (2012).

The actual forearm presented in Figure 7(a) was simplified in terms of the tissues that compose the region and because large blood vessels were also not considered in the analysis [see Figure 7(b), where green, light blue and dark blue represent skin, muscle and bones, respectively]. The values used for the thermal parameters of each tissue are shown by Table I (Hasgall *et al.*, 2015). The convective heat flux at the boundaries was of 10 W $m^{-2^{\circ}}C^{-1}$ and the arterial blood and external medium temperatures were taken as $T_a = 37°C$ and $T_\infty = 20°C$, respectively. Figure 7(b) also presents the region that is assumed to be externally heated as in a hyperthermia treatment of cancer (red circle). The thermal properties for the heated region were considered the same as those selected for the muscle

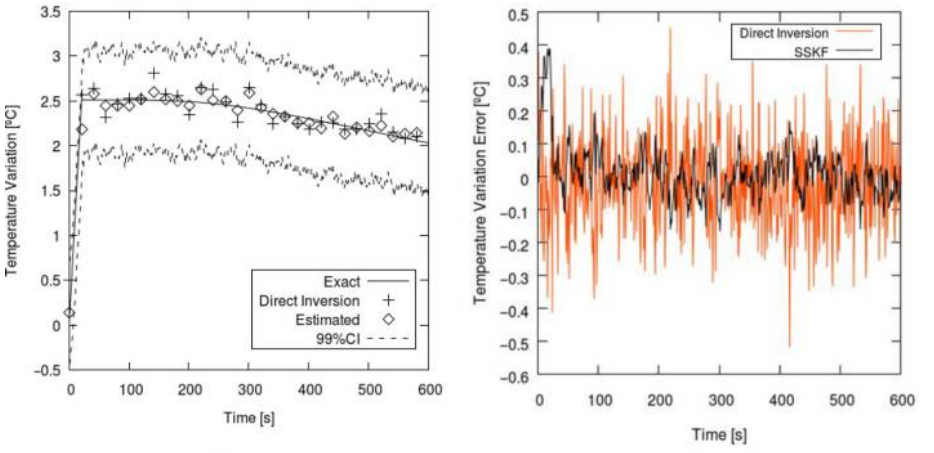

Figure 6.
Time evolution of the results with SSKF and direct inversion at the center of the region ($x = y =$ 0.06 m): (a) temperature variation; and (b) error

region. The external heat source was considered as uniform in this circular region of radius 4 mm, with magnitude $g_h(\mathbf{r},t) = 10^5$ W m^{-3}, and the heating was applied during the whole duration of the experiment, which was 60 s. The magnetic resonance measurements were supposed available every 0.05 s over the same grid used for the solution of the bioheat transfer problem. Uncertainties in the evolution model were taken with a constant standard deviation $\sigma_{\Delta T} = 0.05$°C. Uncertainties in the measurements and observation model also involved a constant standard deviation $\sigma_\delta = 0.2$ degree.

In this problem, the large number of state variables (6,000) resulted in matrices **F**, **H**, **Q** and **R** with 3.6×10^7 elements each. However, due to their nature, these matrices could be handled with fast algorithms appropriate for sparse matrices (Press *et al.*, 1992).

The comparison between the exact values and the SSKF estimates of the temperature variation for the forearm is shown in Figures 8-10, for times $t = 20$ s, 40 s and 60 s, respectively. As for the previous case involving the square region, the agreement between estimated and exact temperature variations is excellent, although some small noise is observed in the region not affected by the source term. Therefore, the SSKF is capable of producing reliable estimates in complex geometries, even with large uncertainties in the measurements and in the evolution/observation models.

The errors in the estimation of the temperature variation, obtained with the direct inversion method and with the SSKF, are shown by Figures 11-13 for $t = 20$, 40 and 60 s, respectively. Similarly to the case involving the square region, the SSKF errors are smaller than those for the direct inversion.

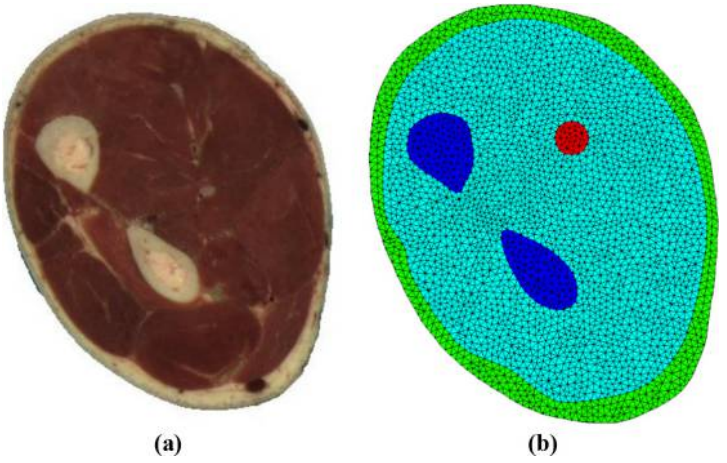

Figure 7.
Transversal cut of right human male forearm: (a) original image, obtained from Spitzer and Whitlock (1998); (b) unstructured grid with triangular control volumes containing skin (green), muscle (light blue) and bone (dark blue) – the red circle represents the heated region

Tissue	k[Wm^{-1}°C^{-1}]	c_p[Jkg^{-1}°C^{-1}]	ρ[kg m^{-3}]	ω/ρ [ml min^{-1}kg^{-1}]	g_m/ρ [W kg^{-1}]v
Skin	0.37	3391	1119	106	1.65
Bone	0.31	2274	1178	30	0.46
Muscle	0.49	3421	1090	37	0.91

Source: Hasgall *et al.* (2015)

Table I.
Thermal properties used for the right forearm geometry

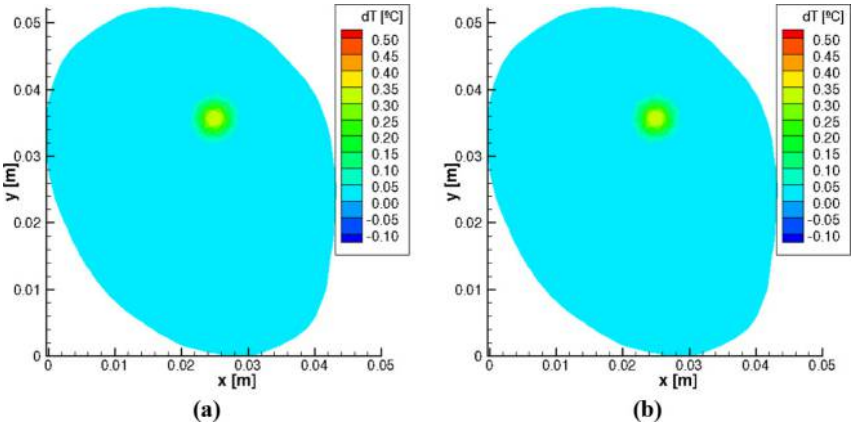

Figure 8.
Temperature variation at $t = 20$ s: (a) exact values; (b) values estimated with SSKF

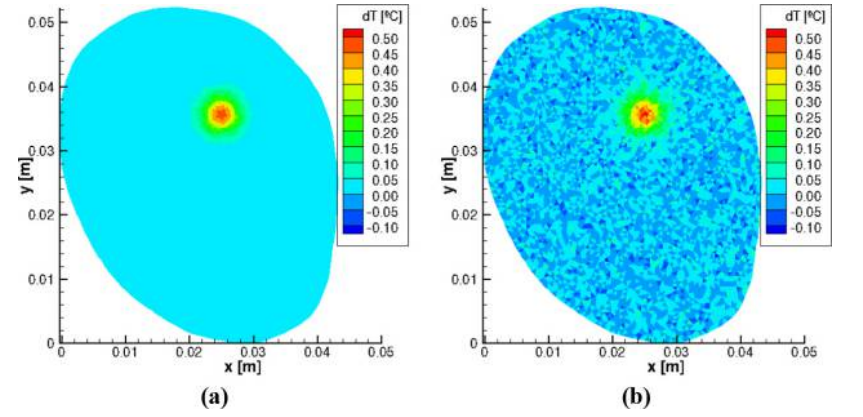

Figure 9.
Temperature variation at $t = 40$ s: (a) exact values; (b) values estimated with SSKF

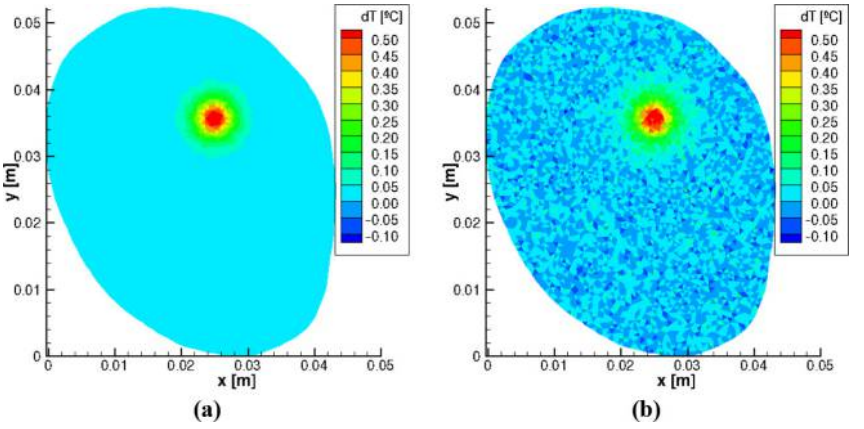

Figure 10.
Temperature variation at $t = 60$ s: (a) exact values; (b) values estimated with SSKF

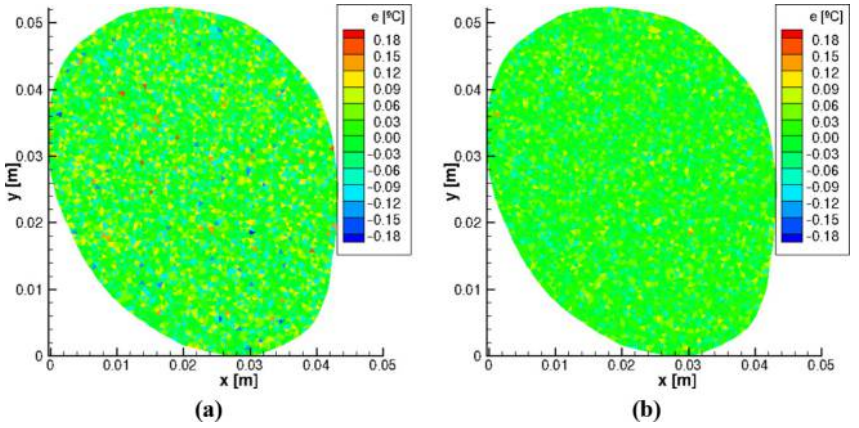

Figure 11.
Absolute error at t = 20 s: (a) direct inversion; (b) SSKF

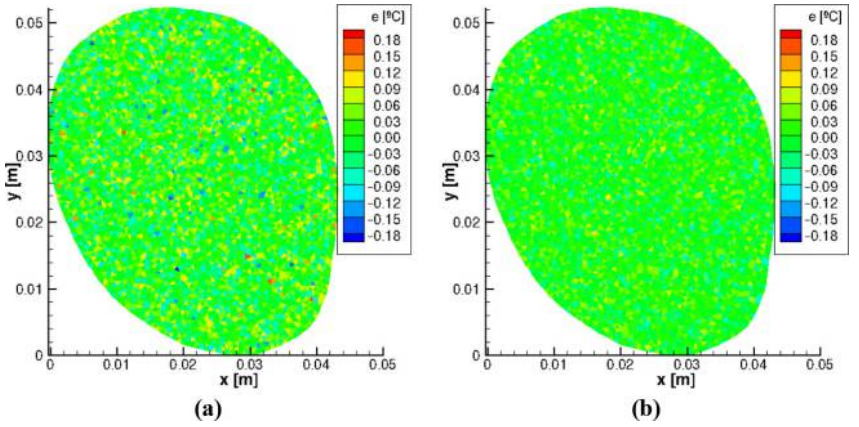

Figure 12.
Absolute error at t = 40 s: (a) direct inversion; (b) SSKF

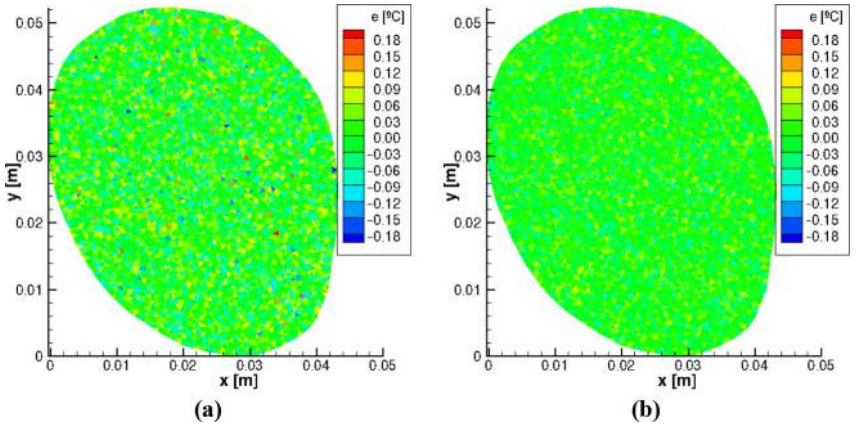

Figure 13.
Absolute error at t = 60 s: (a) direct inversion; (b) SSKF

The time evolution of the temperature variation at the center of the heated region is presented by Figure 14(a). This figure compares exact and estimated values obtained with both inversion methods, where the SSKF estimates are presented with their 99 per cent confidence intervals. One can notice in Figure 14(a) that, as discussed above (Figures 11-13), the estimated temperature variations obtained with SSKF are more accurate than those obtained with the direct inversion. Such conclusion can also be drawn from the analysis of Figure 14(b), which presents the time evolution of the errors between exact and estimated temperature variations. Only the errors at the center of the heated region are presented here for the sake of brevity, but the behavior presented by Figure 14(b) is typical for other points in the domain.

Differently from the direct inversion method that allows for recovering the temperature variation but not the temperature itself, with the approach proposed in this paper, the temperature in the region of interest can be obtained through the solution of the state estimation problem. The estimated temperature fields obtained with the SSKF are shown by Figures 15(b), 16(b) and 17(b), for the times t = 20 s, 40 s and 60 s, respectively. The exact

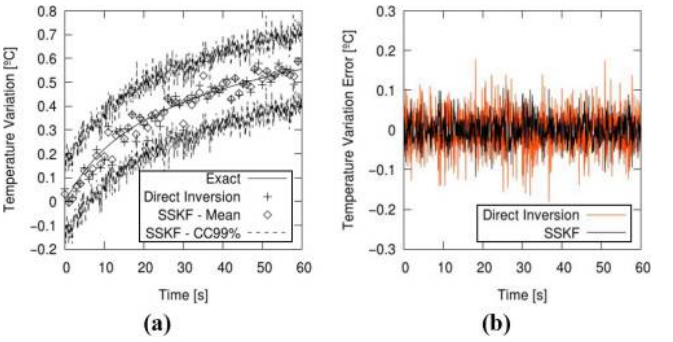

Figure 14.
Results at the center of the heated region: (a) temperature variation; (b) temperature variation error

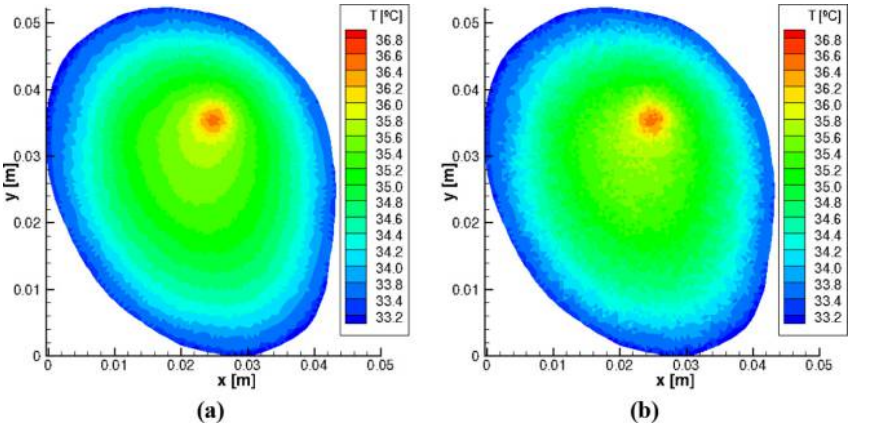

Figure 15.
Temperature at t = 20 s: (a) exact values; (b) values estimated with SSKF

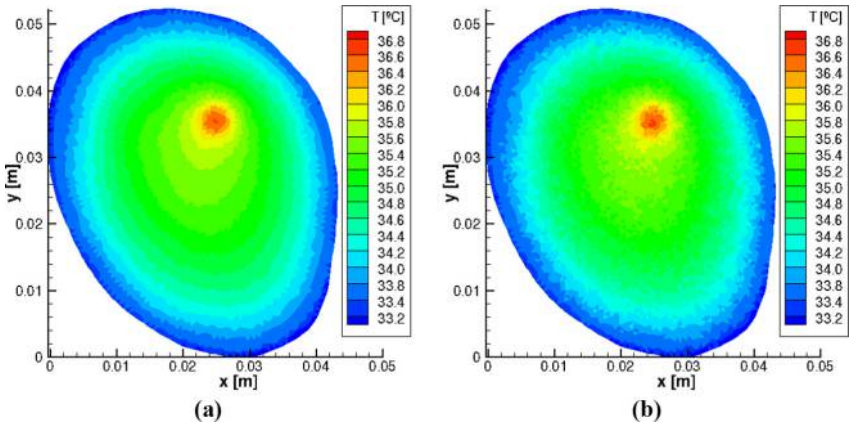

Figure 16.
Temperature at t = 40 s: (a) exact values; (b) values estimated with SSKF

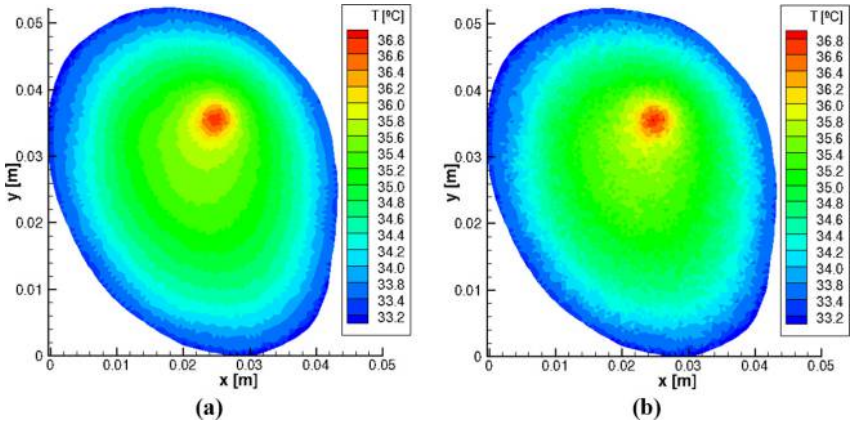

Figure 17.
Temperature at t = 60 s: (a) exact values; (b) values estimated with SSKF

temperature fields for these times are shown by Figures 15(a), 16(a) and 17(a), respectively. For the computation of the estimated temperatures with equation (2), uncorrelated Gaussian noise with zero mean and constant standard deviation of 0.05°C was also added to the solution of problem (3) for $T_0(\mathbf{r})$. Problem (3) was solved over the same grid used for the solution of problem (4). An analysis of Figures 15-17 reveals that the temperature field in the region can be accurately recovered, especially in the region where the heating was applied, which is the most important for the hyperthermia treatment.

In this second case involving the forearm geometry, the recursive estimation via SSKF took around 20 s of computing time, while the preprocessing step required for the solution of Ricatti's equation (16.a) took approximately 6 h. Hence, although the computational time for the solution of Ricatti's equation was significantly affected by the spatial resolution of the problem (that is, the sizes of the matrices in the formulation), the implementation of the recursive equations for SSKF was not. As for the previous case involving the square region, the SSKF can provide estimates of the temperature variation in real time, but with estimation errors much smaller than those obtained from the direct inversion. Furthermore,

the accurate estimation of the temperature field in the region was possible with the solution of the state estimation problem through the SSKF, but not when the direct inversion was used, as demonstrated by Figures 15-17.

Conclusions

In this work, we proposed an approach based on the solution of a state estimation problem for temperature measurements with the PRF-Shift magnetic resonance technique. The state estimation problem was solved with the SSKF. The results obtained with the proposed approach for the temperature variations in two-dimensional regions are compared to those obtained with the direct inversion of the measured data, by using simulated measurements with large uncertainties. Temperature variations estimated with the solution of the state estimation problem are more accurate than those obtained by direct inversion. Besides that, the estimation of the temperature field in the region was possible with the solution of the state estimation problem via the SSKF, but not with the direct inversion. The recursive equations of the SSKF can be calculated in computational times smaller than the supposed physical times, thus demonstrating that the present approach can be used for real-time applications, such as in the control of the heat source for the hyperthermia treatment of cancer.

References

Arulampalam, M.S., Maskell, S., Gordon, N. and Clapp, T. (2002), "A tutorial on particle filters for online nonlinear/non-Gaussian Bayesian tracking", *IEEE Transactions on Signal Processing*, Vol. 50 No. 2, pp. 174-188.

Bayazitoglu, Y. (2009), "Nanoshell-assisted cancer thermal therapy: numerical simulations", *Proceeding 2nd ASME Micro/Nanoscale Heat and Mass Transfer: An International Conference*, December 18-21, Shanghai.

Bayazitoglu, Y., Kheradmand, S. and Tullius, T.K. (2013), "An overview of nanoparticle assisted laser therapy", *International Journal of Heat and Mass Transfer*, Vol. 67, pp. 469-486.

Benner, P., Mehrmann, V., Sima, V., Van Huffel, S. and Varga, A. (1999), "SLICOT-A subroutine library in systems and control theory", in Datta, B. (Ed.), *Applied and Computational Control, Signals, and Circuits SE – 10*, Birkhäuser Boston, pp. 499-539.

Bloch, F. (1946), "Nuclear induction", *Physical Review*, Vol. 70 Nos 7/8, pp. 460-474.

Brown, R.W., Cheng, Y.N., Haacke, E.M., Thompson, M.R. and Venkatesan, R. (1999), *Magnetic Resonance Imaging: Physical Principles and Sequence Design*, Wiley.

Chen, Z. (2003), "Bayesian filtering: from Kalman filters to particle filters, and beyond", *Statistics*, Vol. 182 No. 1, pp. 1-69.

COMSOL (2012), *COMSOL Multiphysics Reference Guide*, COMSOL.

De Poorter, J., De Wagter, C., De Deene, Y., Thomsen, C., Stahlberg, F. and Achten, E. (1994), "The proton-resonance-frequency-shift method compared with molecular diffusion for quantitative measurement of two-dimensional time-dependent temperature distribution in a phantom", *Journal of Magnetic Resonance, Series B*, Vol. 103 No. 3, pp. 234-241.

de Senneville, B.D., Quesson, B. and Moonen, C.T.W. (2005), "Magnetic resonance temperature imaging", *International Journal of Hyperthermia*, Vol. 21 No. 6, pp. 515-531.

De Zwart, J., Vimeux, F., Delalande, C., Canioni, P. and Moonen, C. (1999), "Fast lipid-suppressed MR temperature mapping with echo-shifted gradient- echo imaging and spectral-spatial excitation", *Magnetic Resonance in Medicine*, Vol. 42 No. 1, pp. 53-59.

Dombrovsky, L.A., Timchenko, V., Jackson, M. and Yeoh, G.H. (2011), "A combined transient thermal model for laser hyperthermia of tumors with embedded Gold Nanoshells", *International Journal of Heat and Mass Transfer*, Vol. 54 Nos 25/26, pp. 5459-5469.

Dombrovsky, L.A., Timchenko, V., Pathak, C., Piazena, H., Müller, W. and Jackson, M. (2015), "Radiative heating of superficial human tissues with the use of water-filtered infrared-a radiation: a computational modeling", *International Journal of Heat and Mass Transfer*, Vol. 85, pp. 311-320.

Doucet, A., Smith, A., de Freitas, N. and Gordon, N. (2001), *Sequential Monte Carlo Methods in Practice*, Springer, New York, NY.

Fan, J. and Wang, L. (2011), "Analytical theory of bioheat transport", *Journal of Applied Physics*, Vol. 109 No. 10.

Fiala, D., Havenith, G., Bröde, P., Kampmann, B. and Jendritzky, G. (2012), "UTCI-Fiala multi-node model of human heat transfer and temperature regulation", *International Journal of Biometeorology*, Vol. 56 No. 3, pp. 429-441.

Fite, B.Z., Liu, Y., Kruse, D.E., Caskey, C.F., Walton, J.H., Lai, C.-Y., Mahakian, L.M., Larrat, B., Dumont, E. and Ferrara, K.W. (2012), "Magnetic resonance thermometry at 7T for real-time monitoring and correction of ultrasound induced mild hyperthermia", *PLoS ONE*, Vol. 7 No. 4, p. e35509.

Geuzaine, C. and Remacle, J.-F. (2009), "Gmsh: a 3-D finite element mesh generator with built-in pre- and post-processing facilities", *International Journal for Numerical Methods in Engineering*, Vol. 79 No. 11, pp. 1309-1331.

Grewal, M.S. and Andrews, A.P. (2008), *Kalman Filtering: Theory and Practice Using MATLAB*, Wiley.

Hasgall, P.A., Di Gennaro, F., Baumgartner, C., Neufeld, E., Gosselin, M.C., Payne, D., Klingenböck, A. and Kuster, N. (2015), *IT'IS Database for Thermal and Electromagnetic Parameters of Biological Tissues*, p.Version 3.0., available at: www.itis.ethz.ch/database

Ho, Y.C. and Lee, R. (1964), "A Bayesian approach to problems in stochastic estimation and control", *IEEE Transactions on Automatic Control*, Vol. 9 No. 4, pp. 333-339.

Hynynen, K., Freund, W.R., Cline, H.E., Chung, A.H., Watkins, R.D., Vetro, J.P. and Jolesz, F.A. (1996), "A clinical, noninvasive, MR imaging-monitored ultrasound surgery method", *RadioGraphics*, Vol. 16 No. 1, pp. 185-195.

Ishihara, Y., Calderon, A., Watanabe, H., Okamoto, K., Suzuki, Y., Kuroda, K. and Suzuki, Y. (1995), "A precise and fast temperature mapping using water proton chemical shift", *Magnetic Resonance in Medicine*, Vol. 34 No. 6, pp. 814-823.

Kaipio, J.P. and Somersalo, E. (2004), *Statistical and Computational Inverse Problems*, Springer Science+Business Media.

Kalman, R.E. (1960), "A new approach to linear filtering and prediction problems", *Journal of Basic Engineering*, Vol. 82 No. 1, pp. 35-45.

Kuperman, V. (2000), *Magnetic Resonance Imaging: Physical Principles and Applications*, Elsevier Science.

Kuroda, K., Kokuryo, D., Kumamoto, E., Suzuki, K., Matsuoka, Y. and Keserci, B. (2006), "Optimization of self-reference thermometry using complex field estimation", *Magnetic Resonance in Medicine*, Vol. 56 No. 4, pp. 835-843.

Kuroda, K., Mulkern, R.V., Oshio, K., Panych, L.P., Nakai, T., Moriya, T., Okuda, S., Hynynen, K. and Joles, F.A. (2000), "Temperature mapping using the water proton chemical shift: self-referenced method with echo-planar spectroscopic imaging", *Magnetic Resonance in Medicine*, Vol. 43 No. 2, pp. 220-225.

Lamien, B., Orlande, H.R.B. and Eliçabe, G.E. (2016), "Inverse problem in the hyperthermia therapy of cancer with laser heating and plasmonic nanoparticles", *Inverse Problems in Science and Engineering*, pp. 1-24.

Lamien, B., Varon, L., Orlande, H.R.B. and Eliçabe, G.E. (2017), "State estimation in bioheat transfer: a comparison of particle filter algorithms", *International Journal of Numerical Methods for Heat and Fluid Flow*, Vol. 27 No. 3, pp. 615-638, doi: 10.1108/HFF-03-2016-0118.

Langley, J., Potter, W., Phipps, C., Huang, F. and Zhao, Q. (2011), "A self-reference PRF-shift MR thermometry method utilizing the phase gradient", *Physics in Medicine and Biology*, Vol. 56 No. 24, p. N307.

Mathur, S.R. and Murthy, J.Y. (1997), "A pressure-based method for unstructured meshes", *Numerical Heat Transfer, Part B: Fundamentals*, Vol. 31 No. 2, pp. 195-215.

Mougenot, C., Quesson, B., de Senneville, B.D., de Oliveira, P.L., Sprinkhuizen, S., Palussière, J., Grenier, N. and Moonen, C.T.W. (2009), "Three-dimensional spatial and temporal temperature control with MR thermometry-guided focused ultrasound (MRgHIFU)", *Magnetic Resonance in Medicine*, Vol. 61 No. 3, pp. 603-614.

Mougenot, C., Salomir, R., Palussiere, J., Grenier, N. and Moonen, C.T.W. (2004), "Automatic spatial and temporal temperature control for MR-guided focused ultrasound using fast 3D MR thermometry and multispiral trajectory of the focal point", *Magnetic Resonance in Medicine*, Vol. 52 No. 5, pp. 1005-1015.

Orlande, H.R.B. (2010), "Inverse problems in heat transfer: new trends on solution methodologies and applications", *14th International Heat Transfer Conference - IHTC-14*, August 8-13, Washington, DC.

Orlande, H.R.B., Colaço, M.J., Dulikravich, G.S., Vianna, F.L.V., da Silva, W.B., Fonseca, H.M. and Fudym, O. (2012), "State estimation problems in heat transfer", *International Journal for Uncertainty Quantification*, Vol. 2 No. 3, pp. 239-258.

Ozisik, M.N. (1985), *Heat Transfer: A Basic Approach*, 2nd ed., McGraw-Hill.

Pacheco, C.C., Orlande, H.R.B., Colaço, M.J. and Dulikravich, G.S. (2016), "Real-time identification of a high-magnitude boundary heat flux on a plate", *Inverse Problems in Science and Engineering*, Vol. 24 No. 9, pp. 1661-1679.

Patankar, S.V. (1980), *Numerical Heat Transfer and Fluid Flow*, Hemisphere Publishing Company.

Pennes, H.H. (1948), "Analysis of tissue and arterial blood temperatures in the resting human forearm", *Journal of Applied Physiology*, Vol. 1 No. 2, pp. 93-122.

Press, W., Flannery, B., Teukolsky, S. and Vetterling, W. (1992), *Numerical Recipes in Fortran: The Art of Scientific Computing*, Cambridge University Press.

Quesson, B., De Zwart, J.A. and Moonen, C.T.W. (2000), "Magnetic resonance temperature imaging for guidance of thermotherapy", *Journal of Magnetic Resonance Imaging*, Vol. 12 No. 4, pp. 525-533.

Rieke, V. and Butts Pauly, K. (2008), "MR thermometry", *Journal of Magnetic Resonance Imaging*, Vol. 27 No. 2, pp. 376-390.

Rieke, V., Vigen, K.K., Sommer, G., Daniel, B.L., Pauly, J.M. and Butts, K. (2004), "Referenceless PRF shift thermometry", *Magnetic Resonance in Medicine*, Vol. 51 No. 6, pp. 1223-1231.

Salomir, R., de Senneville, B.D. and Moonen, C.T. (2003), "A fast calculation method for magnetic field inhomogeneity due to an arbitrary distribution of bulk susceptibility", *Concepts in Magnetic Resonance*, Vol. 19B No. 1, pp. 26-34, available at: http://doi.wiley.com/10.1002/cmr.b.10083

Salomir, R., Vimeux, F.C., de Zwart, J.A., Grenier, N. and Moonen, C.T. (2000a), "Hyperthermia by MR-guided focused ultrasound: accurate temperature control based on fast MRI and a physical model of local energy deposition and heat conduction", *Magnetic Resonance in Medicine*, Vol. 43 No. 3, pp. 342-347.

Salomir, R., Palussire, J., Vimeux, F.C., De Zwart, J.A., Quesson, B., Gauchet, M., Lelong, P., Pergrale, J., Grenier, N. and Moonen, C.T.W. (2000b), "Local hyperthermia with MR-guided focused ultrasound: spiral trajectory of the focal point optimized for temperature uniformity in the target region", *Journal of Magnetic Resonance Imaging*, Vol. 12 No. 4, pp. 571-583.

Simon, D. (2006), *Optimal State Estimation: Kalman, H Infinity, and Nonlinear Approaches*, John Wiley & Sons.

Spitzer, V.M. and Whitlock, D.G. (1998), "The visible human dataset: the anatomical platform for human simulation", *The Anatomical Record*, Vol. 253 No. 2, pp. 49-57.

Varon, L.A.B., Orlande, H.R.B. and Eliçabe, G.E. (2015), "Estimation of state variables in the hyperthermia therapy of cancer with heating imposed by radiofrequency electromagnetic waves", *International Journal of Thermal Sciences*, Vol. 98, pp. 228-236.

Varon, L.A.B., Orlande, H.R.B. and Eliçabe, G.E. (2016), "Combined parameter and state estimation in the radio frequency hyperthermia treatment of cancer", *Numerical Heat Transfer, Part A: Applications*, Vol. 70 No. 6, pp. 581-594.

Versteeg, H.K. and Malalasekera, W. (1995), *An Introduction to Computational Fluid Dynamics: The Finite Volume Method*, Longman Group Ltd.

Weidensteiner, C., Kerioui, N., Quesson, B., de Senneville, B.D., Trillaud, H. and Moonen, C.T.W. (2004), "Stability of real-time mr temperature mapping in healthy and diseased human liver", *Journal of Magnetic Resonance Imaging*, Vol. 19 No. 4, pp. 438-446.

Wlodarczyk, W., Boroschewski, R., Hentschel, M., Wust, P., Mönich, G. and Felix, R. (1998), "Three-dimensional monitoring of small temperature changes for therapeutic hyperthermia using MR", *Journal of Magnetic Resonance Imaging*, Vol. 8 No. 1, pp. 165-174.

Yang, Q.X., Williams, G.D., Demeure, R.J., Mosher, T.J. and Smith, M.B. (1998), "Removal of local field gradient artifacts in T2*-weighted images at high fields by gradient-echo slice excitation profile imaging", *Magnetic Resonance in Medicine*, Vol. 39 No. 3, pp. 402-409.

Corresponding author
Helcio R.B. Orlande can be contacted at: helcio@mecanica.coppe.ufrj.br